Possible Role of a PXXP Central Hinge in the Antibacterial Activity and Membrane Interaction of PMAP-23, a Member of Cathelicidin Family†

Sung-Tae Yang,‡ Jae-Hyuck Jeon,§ Yangmee Kim,|| Song Yub Shin,⊥ Kyung-Soo Hahm,⊥ and Jae Il Kim*,‡

Department of Life Science, Gwangju Institute of Science and Technology, Gwangju 500-712, Korea, AnyGen Co., Ltd., 598-1 Daechon-dong, Puk-gu Gwangju 500-470, Korea, Department of Chemistry, Konkuk University, Seoul 143-701, Korea, and Department of Bio-Materials, Graduate School and Research Center for Proteineous Materials, Chosun University, Gwangju 501-759, Korea

Received August 1, 2005; Revised Manuscript Received December 14, 2005

ABSTRACT: Cathelicidins are essential components of the innate immune system of mammals, providing them a weapon against microbial invasion. PMAP-23 adopting a helix−hinge−helix structure with a central PXXP motif is a member of the cathelicidin family and has potent killing activities against a broad spectrum of microbial organisms. Although the antimicrobial effect of PMAP-23 is believed to be mediated by membrane disruption, many details of this event remain unclear. Here, we try to characterize the interaction between PMAP-23 and membrane phospholipids, focusing on the function of the central PXXP motif. PMAP-PA, in which the Pro residues were substituted by Ala, had significantly more α-helical content than PMAP-23, but was less amphipathic and more damaging to human erythrocytes and zwitterionic liposomes. The observed differences in the structures and biological activities of PMAP-23 and PMAP-PA confirmed the functional importance of the central hinge PXXP motif, which enables PMAP-23 to adopt a well-defined amphipathic conformation along its entire length and to have selective antimicrobial activity. CD and Trp fluorescence studies using fragments corresponding to the two helical halves of PMAP-23 revealed that the N-terminal half binds to anionic phospholipids and is more stable than the C-terminal half. In addition, Trp fluorescence quench analyses revealed that the C-terminal helix inserts more deeply into the hydrophobic region of the membrane than the N-terminal helix. Finally, observations made using biosensor technology enabled us to distinguish between the membrane binding and insertion steps, substantiating a proposed kinetic mode of the peptide-membrane interaction in which PMAP-23 first attaches to the membrane via the N-terminal amphipathic helix, after which bending and/or swiveling of the PXXP motif enables insertion of the C-terminal helix into the lipid bilayer.

Natural antimicrobial peptides are widely distributed among multicellular organisms and are known to play crucial roles in nonspecific host defense and innate immunity (*1*−*4*). In mammals, the cytoplasmic granules of neutrophils are an abundant source for a number of such host defensive peptides, a major of class which is the cathelicidin family, which contains a highly conserved N-terminal domain called cathelin-like and an extremely diverse antimicrobial C-terminal domain (*5*−*7*). Despite the remarkable diversity of their primary sequences, the cathelicidin-derived peptides have been grouped into α-helical, Cys-rich, Pro/Arg-rich, and Trp-rich subfamilies based on their common structural features (*8*, *9*). Most of these peptides are effective against a broad spectrum of targets, including bacteria, fungi, parasites, and even tumor cells (*10*, *11*). Although the precise mechanism by which they kill pathogens is not fully understood, most are known to be membrane-active molecules that kill microorganisms through membrane disruption (*12*). Consequently, their mechanisms of action, potencies, and specificities often have been studied by examining their interactions with various model membranes, and it is now well established that these peptides exhibit a structural transition from an extended coil to a well-defined secondary structure upon binding to membrane surfaces (*13*, *14*). Moreover, the folded structures tend to be highly amphipathic, with basic and hydrophobic amino acids segregated into distinct regions of the molecular surface. This amphipathic structure allows the basic portions of the peptides to interact with a variety of bacterial membranes, which are largely comprised of anionic phospholipids, resulting in wide-spectrum antibiotic activity (*13*, *14*). The fact that these peptides exhibit little or no binding to zwitterionic phospholipids, which are the major component of the outer leaflet of hRBCs[1] (*15*, *16*), likely explains their specificity for prokaryotic cell membranes (*17*). Still, little detailed information about the associated structural changes and kinetics

† This study was supported by the SRC/ERC program of MOST/KOSEF (R11-2000-083-00000-0), the Molecular and Cellular BioDiscovery Research Program, the Brain Research Center of the 21st Century Frontier Research Program (M103KV010004 03K2201 00430), and the Development of Marine Novel Compounds Program of the Korean Ministry of Maritime Affairs and Fisheries. S.-T.Y. is supported in part by the Korean Ministry of Education (Brain Korea 21 program).

* To whom all correspondence should be addressed. Tel: 82-62-970-2494. Fax: 82-62-970-2484. E-mail: jikim@gist.ac.kr.

‡ Gwangju Institute of Science and Technology.

§ AnyGen Co., Ltd.

|| Konkuk University.

⊥ Chosun University.

10.1021/bi051524k CCC: $33.50
Published on Web 01/17/2006

of the peptide-membrane interaction are available for these molecules.

PMAP-23 (RIIDLLWRVRRPQKPKFVTVWVR) is a member of the cathelicidin family and was identified from the cDNA of porcine myeloid mRNA (*18*). Intrinsically fluorescent due to the presence of two Trp residues, PMAP-23 is a convenient model for monitoring peptide−membrane interactions. The peptide shows a broad spectrum of antimicrobial activity against both Gram-positive and Gram-negative bacteria, as well as fungi, but it has no hemolytic activity, even at a concentration of 100 μM (*18*, *19*). Indeed, its potency and selectivity make PMAP-23 a highly attractive candidate for developing new antibiotics to treat infections caused by multidrug-resistant microorganisms. Our earlier NMR spectroscopic analysis showed that PMAP-23 adopts a unique helix−hinge−helix structure in membrane-mimetic environments; i.e., it consists of N-terminal (residues 1−10) and C-terminal (residues 17−23) α-helical regions connected by a flexible hinge region containing a PXXP motif (*20*). In addition, our confocal laser scanning microscopic observations and FACScan analyses suggest PMAP-23 localizes to and then disrupts plasma membranes by inducing ion channel or pore formation (*21*). But while the association of PMAP-23 with the membrane is obviously linked to its physiological effects, details of the interaction of the peptide with the various membrane components remain unknown. Moreover, it is clear that understanding the peptide−lipid interaction, including the structural changes that occur within the phospholipid bilayer, could aid in the rational design of novel antibiotics for clinical use. Our aim in the present study, therefore, was to begin to characterize the respective functions of the central PXXP motif and the N- and C-terminal helices of PMAP-23 and to model the orientation of the peptide adopting a helix−hinge−helix structure in the presence of lipid bilayer so as to better understand its mode of action.

MATERIALS AND METHODS

Peptide Synthesis and Purification. The peptides were synthesized using the solid-phase method with Fmoc (*22*). Fmoc-protected peptides were deprotected and cleaved by incubation with a mixture of trifluoroacetic acid, phenol, water, thioanisole, and 1, 2-ethandithiol (82.5:5:5:5:2.5, v/v) for 3 h at room temperature. The synthetic peptides were purified by RP-HPLC on Shimadzu LC-6AD and Shimadzu LC-10Avp systems using an ODS column (4.6 × 250 mm). The purified peptides were shown to be homogeneous (~98%) by analytical HPLC. The molecular weight of all synthetic peptides was confirmed using Kratos Kompact matrix-assisted laser desorption/ionization time-of-flight mass spectrometry (MALDI-TOF MS, Shimadzu, Japan).

Microorganisms and Antimicrobial Activity. Escherichia coli KCTC 1682, *Enterococcus faecalis* KCTC2011, *Pseudomonas aeruginosa* KCTC 1637, *Bacillus subtilis* KCTC 3068, and *Staphylococcus aureus* KCTC 1621 were purchased from the Korean Collection for Type Cultures and the Korea Research Institute of Bioscience & Biotechnology (Daejon, Korea). The antimicrobial activity of the peptides against Gram-positive and Gram-negative bacteria was determined using broth microdilution assays. Briefly, single colonies of bacteria were inoculated into LB broth medium and cultured overnight at 37 °C. An aliquot of this culture was then transferred to 10 mL of fresh culture medium and incubated for an additional 3−5 h at 37 °C to obtain mid-logarithmic phase organisms. A 2-fold dilution series of peptides in 1% peptone was prepared, and a set of serial dilutions (100 μL) was added to 100 μL of 2×10^6 CFU/ml in 96-well microtiter plates (Falcon) and incubated at 37 °C for 16 h. The lowest peptide concentration that completely inhibited the growth of the organisms was defined as the MIC. The recorded MICs were the average of triplicate measurements in three independent assays.

Hemolytic Activity. The hemolytic activities of the peptides were determined using hRBCs. The hRBCs were centrifuged and washed three times with PBS (35 mM phosphate buffer, pH 7.0/150 mM NaCl), after which 100 μL of 4% (v/v) hRBCs (suspended in PBS) was dispensed into sterilized 96-well plates and 100 μL of the peptide solution was added to each well. After incubating for 1 h at 37 °C, the cells were collected and centrifuged at 1000*g* for 5 min, and aliquots (100 μL) of the supernatant were transferred to 96-well plates, where hemoglobin release was monitored by measuring the absorbance at 414 nm using an ELISA plate reader (Molecular Devices, Sunnyvale, CA). Percent hemolysis was calculated using the following formula: % hemolysis = [($Abs_{414\ nm}$ in the peptide solution − $Abs_{414\ nm}$ in PBS)/($Abs_{414\ nm}$ in 0.1% Triton-X 100 − $Abs_{414\ nm}$ in PBS)] × 100. Zero and 100% hemolysis were determined in PBS and 0.1% Triton X-100, respectively. The recorded hemolysis (%) was the average of duplicate measurements in three independent assays.

Preparation of Small and Large Unilamellar Vesicles. Small unilamellar vesicles were prepared for CD and SPR experiments by sonication. Phospholipids composed of POPC/POPG (2:1) were dissolved in chloroform and dried with a stream of nitrogen to form a thin lipid film. The lipid film was then dried under vacuum overnight and resuspended in 20 mM sodium phosphate buffer via vortex mixing. The resultant suspension was sonicated under nitrogen in an ice bath for about 20 min using a titanium-tipped sonicator until clear. Dynamic light-scattering experiments confirmed the existence of a main population of vesicles (more than 96% mass content) with a mean diameter of 42 nm. Large unilamellar vesicles were prepared for fluorescence release experiments by extrusion. Dried lipid film composed of POPC, POPC/POPG (2:1), or POPG was hydrated with Tri-HCl buffer (10 mM Tris−HCl, pH 7.4, 150 mM NaCl, 0.1 mM EDTA) or a 70 mM calcein solution and vortex-mixed. The resultant suspension was freeze−thawed for five cycles and then successively extruded 20 times through polycarbonate filters (LiposoFast, pore diameter 100 nm). Calcein-entrapped vesicles were separated from free calcein by gel filtration chromatography on a Sephadex G-50 column using Tris−HCl buffer.

CD Spectroscopy. The CD spectra of the peptides were recorded using a JASCO J-715 CD spectrophotometer

[1] Abbreviations: CD, circular dichroism; Fmoc, fluoren-9-yl-methoxycarbonyl chemistry; hRBC, human red blood cells; MALDI-TOF MS, matrix-assisted laser desorption/ionization time-of-flight mass spectrometry; MIC, minimal inhibitory concentration; POPC, 1-palmitoyl-2-oleoylphosphatidylcholine; POPG, 1-palmitoyl-2-oleoylphosphatidylglycerol; RP-HPLC, reversed-phase high-performance liquid chromatography; SPR, surface plasmon resonance; SH3, Src homology 3.

(Tokyo, Japan) with a 1 mm path length cell. Wavelengths from 190 to 250 nm were measured at 50 nm/min; the step resolution was 0.1 nm, the response time 0.5 s, and the bandwidth 1 nm. The CD spectra of the peptides were collected and averaged over four scans in 20 mM sodium phosphate buffer (pH 7.0) or in 2 mM POPC/POPG (2:1) liposomes at 25 °C. The mean residue ellipticity $[\theta]$ (given in deg·cm^2·dmol^{-1}) was calculated as $[\theta] = [\theta]$obs (MRW/10*lc*), where $[\theta]$obs is the ellipticity measured in millidegrees, MRW is the mean residue molecular weight of the peptide, *c* is the concentration of the sample in mg/mL, and *l* is the optical path length of the cell in cm. The spectra are expressed as molar ellipticity $[\theta]$ vs wavelength. The helical contents were calculated using the equation % α-helical content $= 100\ ([\theta]_{222} - [\theta]^0_{222})/[\theta]^{100}_{222}$, where $[\theta]_{222}$ is experimentally observed ellipticity at 222 nm. Values of −30300 and −2340 were taken for 100% ($[\theta]^{100}_{222}$) and 0% ($[\theta]^0_{222}$) helix content, respectively.

Calcein Release Assays. The fluorescence intensity of calcein released from liposomes was monitored at 520 nm (excited at 490 nm) on a Shimadzu RF-5301 spectrofluorometer. To measure the maximum fluorescence intensity for 100% dye-leakage, 20 μL of Triton X-100 (20% in Tris buffer) was added to dissolve the vesicles. The average percentage (by three independent assays) of dye-leakage caused by the peptides was calculated using the equation % leakage $= 100(F - F_0)/(F_t - F_0)$, where F_0 and F_t are the initial fluorescence intensities observed without the peptides and after Triton X-100 treatment, respectively, and *F* is the fluorescence intensity achieved with the peptides.

Tryptophan Fluorescence and Quenching by Acrylamide. Tryptophan fluorescence measurements were made on a Shimadzu RF-5301 spectrofluorometer. Each peptide (3 μM) was added to 3 mL of 10 mM Tris−HCl buffer (pH 7.4) containing 300 μM liposomes, and the peptide/liposome mixture was allowed to interact at 25 °C for 10 min. Trp fluorescence was then excited at 280 nm, and the emission was scanned from 300 to 400 nm. For fluorescence quenching experiments, Trp was excited at 295 nm instead of 280 nm to reduce absorbance by acrylamide. Trp fluorescence was quenched by titration of acrylamide from a 4 M stock solution to the final concentration of 0.2 M in the presence of liposome at a peptide/lipid molar ratio of 1:100 (The concentrations of peptides and phospholipid vesicles were 3 and 300 μM, respectively.) Experimental data were plotted according to the Stern−Volmer equation $F_0/F = 1 + K_{SV}$[Q], where F_0 is the fluorescence of the peptide in the absence of acrylamide, *F* is the fluorescence of the peptide in the presence of acrylamide, K_{SV} is the Stern−Volmer quenching constant, and [Q] is the concentration of acrylamide. Measurements were repeated three times at a given condition to ensure reproducibility.

Analysis of Peptide−Membrane Interactions Using SPR. The interaction of PMAP-23 and PMAP-PA with the phospholipid membrane was analyzed by SPR using a BIACORE 2000 equipped with an L1 sensor chip. The running buffer used for all experiments was 20 mM sodium phosphate buffer. The L1 sensor chip was installed and washed with 40 mM *N*-octyl β-D-glucopyranoside (25 μL) at a flow rate of 5 μL/min. POPC/POPG (2:1) small unilamellar vesicles were then immediately applied to the chip surface for 15 min at a flow rate of 2 μL/min. To remove any multilamellar structures from the lipid surface or to regenerate the surface, 10 mM sodium hydroxide (50 μL) was injected at flow rate of 50 μL/min, which resulted in a stable baseline. BSA was injected (25 μL, 0.1 mg/μL in sodium phosphate buffer) as a negative control; complete coverage of the chip surface with lipid was confirmed by the absence of nonspecific BSA binding. All experiments were carried out at 25 °C, and all solutions were freshly prepared, degassed, and filtered through 0.22 μm pores. Measurements were repeated two times under the given conditions to ensure reproducibility. The sensorgrams for each peptide−lipid interaction were analyzed by curve fitting using numerical integration analysis (*23*). The data were fitted globally by simultaneously fitting the peptide sensorgrams obtained at seven different concentrations using BIA evaluation software (version 3.2). Because a poor fit was obtained with the simple 1:1 binding model, a two-state reaction model was applied to the sensorgrams to determine the association and dissociation rate constants. This model describes two reaction steps, which with regard to peptide−lipid interaction may correspond to

$$P + L \underset{k_{d1}}{\overset{k_{a1}}{\leftrightarrow}} PL \underset{k_{d2}}{\overset{k_{a2}}{\leftrightarrow}} PL^*$$

where peptide (P) initially binds to lipids (L) to give the complex PL as a result of initial electrostatic binding. In the second step, PL changes to PL*, which cannot dissociate directly to P + L and which may correspond to the insertion of the peptide into the hydrophobic region of the lipid bilayer. The corresponding differential rate equations for this reaction model are represented by

$$dR_1/dt + k_{a1}C_A(R_{max} - R_1 - R_2) - k_{d1}R_1 - k_{a2}R_2 + k_{d2}R_2$$

$$dR_2/dt = k_{a2}R_1 - k_{d2}R_2$$

where R_1 and R_2 are the response units for the first and second steps, respectively, C_A is the peptide concentration, and R_{max} is the maximal response unit (or equilibrium binding response). The total affinity constant (*K*) was determined as (k_{a1}/k_{d1}) (k_{a2}/k_{d2}).

RESULTS

Design and Synthesis of the Peptides. PMAP-23 consists of two amphipathic α-helices separated by an unstructured hinge region incorporating two Pro residues (Figure 1*A* and *B*) (*21*). To investigate the effect of the central hinge formed by the PXXP motif on the peptide's structure, antibiotic activity, and membrane interaction, we synthesized a Pro→Ala substitution analogue (PMAP-PA). In addition, to examine how the N- and C-terminal helical portions of PMAP-23 are involved in membrane binding and disruption, we synthesized NF-PMAP and CF-PMAP, which are, respectively, comprised of the 11 amino acids corresponding to the N- and C-terminal halves of PMAP-23. The presence of a Trp residue in each of its helical halves—Trp^7 is positioned in the center of the N-terminal helix, while Trp^{21} is positioned at the end of the C-terminal helix—enables PMAP-23 to serve as a convenient model with which to monitor peptide membrane interactions. Finally, to gain better insight into

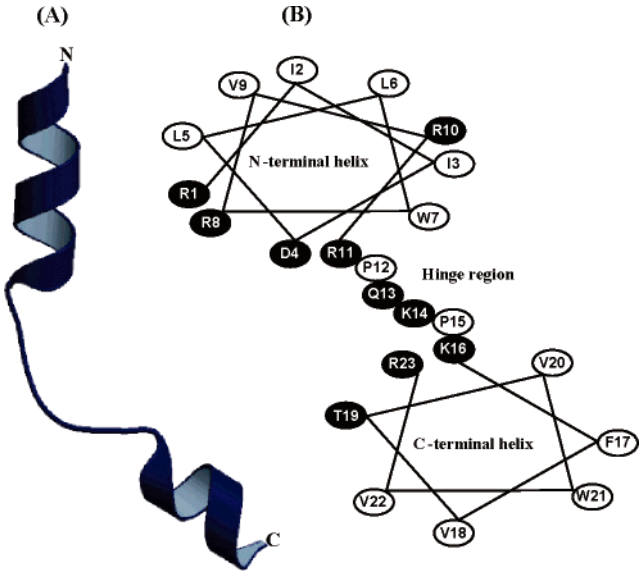

(C)

PMAP-23	RIIDLLWRVRRPQKPKFVTVWVR
PMAP-PA	RIIDLLWRVRR**A**QK**A**KFVTVWVR
NF-PMAP	RIIDLLWRVRR
CF-PMAP	QKPKFVTVWVR
PMAP-W_7F_{21}	RIIDLLWRVRRPQKPKFVTV**F**VR
PMAP-F_7W_{21}	RIIDLL**F**RVRRPQKPKFVTVWVR

FIGURE 1: (A) Ribbon-model representation of the backbone structure of PMAP-23 (reprinted with permission from ref 20). PMAP-23 has a helix-hinge-helix structure with an overall amphipathic structure. (B) Helical wheel diagram of PMAP-23. Black circles refer to charged or hydrophilic amino acids, white circles to hydrophobic residues. (C) Amino acid sequences of PMAP-23 and its analogues used in this study.

the orientation of the helix−hinge−helix structure in the membrane, we synthesized two single Trp analogues, PMAP-W_7F_{21} and PMAP-F_7W_{21}. The amino acid sequences of wild-type PMAP-23 and the analogues used are presented in Figure 1C. The correct molecular weights of all the synthetic peptides were confirmed by MALDI-MS.

Structural Analysis of the Peptides Using CD Spectroscopy. The secondary structures of wild-type PMAP-23 and its analogues in 20 mM sodium phosphate buffer with and without 2 mM POPC/POPG (2:1) liposomes were analyzed using CD spectroscopy. All of the peptides exhibited negative bands below 200 nm in aqueous buffer (data not shown), indicating the absence of regular structure, but assumed an ordered conformation in the presence of the liposomes. The spectra of PMAP-23 and the indicated analogues along with their respective α-helical contents in the presence of anionic liposomes are shown in Figure 2. PMAP-23 showed a strong negative band at 204 nm, which is indicative of a conformation that is somewhat different from a typical α-helix and likely reflects the flexible region of the peptide. Very similar CD spectral patterns were also observed with the two single Trp-containing analogues (data not shown). On the other hand, PMAP-PA showed a typical α-helical CD pattern, with minimal mean residue molar ellipticity values of 207 and 222 nm. Thus, Pro→Ala substitution at the central position of PMAP-23 markedly increased its α-helical content, suggesting that whereas PMAP-23 adopts two distinct amphipathic α-helices separated by an unstructured hinge region, PMAP-PA likely consists of a single long α-helix.

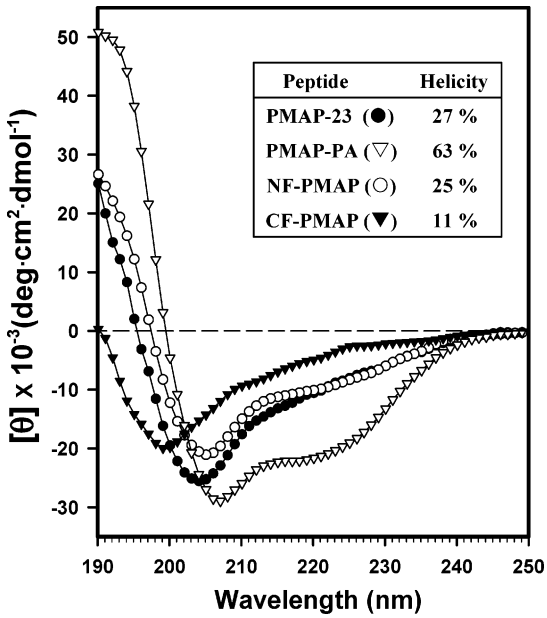

FIGURE 2: CD spectra of PMAP-23, PMAP-PA, PMAP-NF, and PMAP-CF. Spectra were taken at a peptide concentration of 20 μM in 2 mM POPC/POPG (2:1) liposomes. Symbols: PMAP-23 (●); PMAP-PA (▽); NF-PMAP (○); CF-PMAP (▼). The inset shows the α-helical content of the peptides. Data are representative of two independent experiments.

Moreover, the α-helical wheel diagram of PMAP-PA shows that the hydrophobic amino acids are not separated from the hydrophilic ones, making PMAP-PA significantly less amphipathic than PMAP-23. The CD spectrum of the N-terminal half of PMAP-23 (NF-PMAP) is similar to that of full-length peptide, though the intensity of the molar ellipticity was somewhat reduced. By contrast, the C-terminal half (CF-PMAP) had no distinct secondary structure, with a broad negative band at about 200 nm. That the C-terminal region of the full peptide contains a short α-helical structure while the C-terminal fragment has a disordered structure suggests that the initial N-terminal interaction with the membrane proceeds to a second state in which the C-terminal α-helix elongates.

Comparison of the Antibacterial and Hemolytic Activities of the Peptides. We next evaluated the antimicrobial activity of PMAP-23 and its analogues against Gram-negative and Gram-positive bacteria and their lytic activity against hRBCs. Listed in Table 1 are the antimicrobial activities of the peptides expressed in MICs and their hemolytic activity expressed as % lysis of hRBCs. PMAP-23, PMAP-W_7F_{21}, and PMAP-F_7W_{21} showed a similar potency toward all tested microorganisms, with MICs ranging from 2 to 16 μM, but they exerted virtually no hemolytic effect. PMAP-PA, by contrast, showed 2−4 times less potent antibacterial activity but somewhat more hemolytic activity (16.3% hemolysis with a deviation not exceeding 4% at 128 μM). The N-terminal fragment was about 4−16 times less active than PMAP-23, and the C-terminal fragment was nearly inactive. Collectively, these findings suggest that the potency and selectivity of PMAP-23's antimicrobial activity is largely dependent on the central PXXP motif, and that the increased α-helicity and reduced amphipathicity of PMAP-PA is related to its increased hemolytic and reduced antibacterial activity.

Table 1: MICs (μM)[a] and Hemolytic Activities of PMAP-23 and Its Analogues

cells	PMAP-23	PMAP-PA	NF-PMAP	CF-PMAP	PMAP-W_7F_21	PMAP-F_7W_21
bacterial cells						
E. coli	2−4	8−16	16−32	NA[b]	4	2−4
P. aeruginsa	4−16	8−16	64	NA	8−16	4−16
E. faecalis	4−8	16	32	NA	8	4−8
B. subtilis	2	8	16−32	128	2−4	2
S. aureus	4	8−16	16−32	128	4	4
hRBCs						
% hemolysis[c]	NA	16.3	NA	NA	NA	NA

[a] Results are the range of three independent experiments, each performed in triplicate. [b] NA, not active up to 128 μM. [c] The hemolytic activity was performed at 128 μM.

Peptide-Induced Calcein Release from Liposomes. The capacities of PMAP-23 and its analogues to disrupt membranes were compared by assessing their ability to induce release of entrapped calcein from liposomes made up of zwitterionic POPC, highly anionic POPG, or a 2:1 mixture of POPC and POPG. The relative lytic efficiencies with standard deviation not exceeding 12% were determined by comparison with Triton X-100, which induced complete disruption. When added to POPC liposomes, PMAP-23, NF-PMAPm and CF-PMAP elicited no calcein release even at peptide concentrations up to 60 μM, whereas PMAP-PA elicited 21% release at 50 μM, further suggesting a positive correlation between its disruption of zwitterionic liposomes and its hemolytic activity (Figure 3A). PMAP-23 showed the most potent membrane-disrupting activity against the anionic POPC/POPG and POPG liposomes, inducing almost total release of calcein from POPG liposomes at a concentration of 2 μM (Figure 3B,C). PMAP-23, PMAP-W_7F_{21}, and PMAP-F_7W_{21} showed similar potency toward all tested liposome types (data not shown). That NF-PMAP and CF-PMAP showed significantly less activity (68% and 25% release at 10 μM, respectively) than the full-length peptide suggests the overall helix−hinge−helix structure of PMAP-23 is required for the full expression of its selective activity against anionic membranes.

Peptide Binding to Model Membranes. The presence of two Trp residues makes PMAP-23 intrinsically fluorescent and a useful probe with which to study peptide−membrane interactions, as the emission maximum of each Trp residue varies depending upon its environment. We monitored Trp fluorescence in buffer with and without POPC, POPC/POPG (2:1) or POPG liposomes (Figure 4 and Table 2). In Tris buffer, the wavelength maxima of the peptides were in the range of 352−353 nm, indicating the Trp residues to be located in a hydrophilic environment. When POPC liposomes were added to buffer containing PMAP-23, there was no change the Trp fluorescence spectrum. By contrast, addition of POPC liposomes to PMAP-PA elicited a small (5 nm) blue shift and an increase in the intensity of the Trp fluorescence maximum, indicating movement of the residue from the aqueous environment of the buffer to a more hydrophobic environment. Upon addition of POPC/POPG (2:1) or POPG liposomes, the fluorescence emission maxima of both PMAP-23 and PMAP-PA were shifted to shorter wavelengths and increased in intensity, again indicating movement of Trp from an aqueous to a hydrophobic environment. Interestingly, in the presence of POPG liposomes, the fluorescence spectrum of PMAP-23 displayed a larger blue shift than that of PMAP−PA, indicating movement of Trp deeper into the hydrophobic region of the membrane. Addition of NF-PMAP to POPG liposomes gave rise to a smaller blue shift (8 nm), while CF-PMAP showed only a negligible shift, indicating that the major driving force for PMAP-23 binding to membranes is the attractive electrostatic interaction between the negatively charged lipid headgroups and the positively charged amino acids in the N-terminal region in PMAP-23. Of the two single Trp mutants, PMAP-F_7W_{21} showed a larger blue shift than PMAP-W_7F_{21} (14 nm vs 10 nm), indicating that Trp^{21} in the

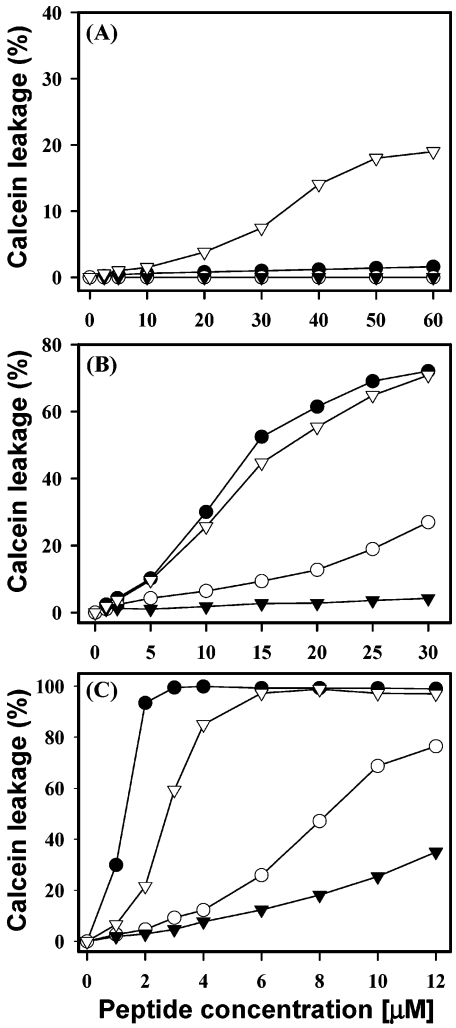

FIGURE 3: Dose-dependent leakage of calcein from liposomes. Calcein release from POPC (A), POPC/POPG (2:1) (B), and POPG (C) liposomes was defined as the percent release after 5 min at a lipid concentration of 70 μM. Symbols: PMAP-23 (●); PMAP-PA (▽); NF-PMAP (○); CF-PMAP (▼). Each data point is the mean of three independent experiments.

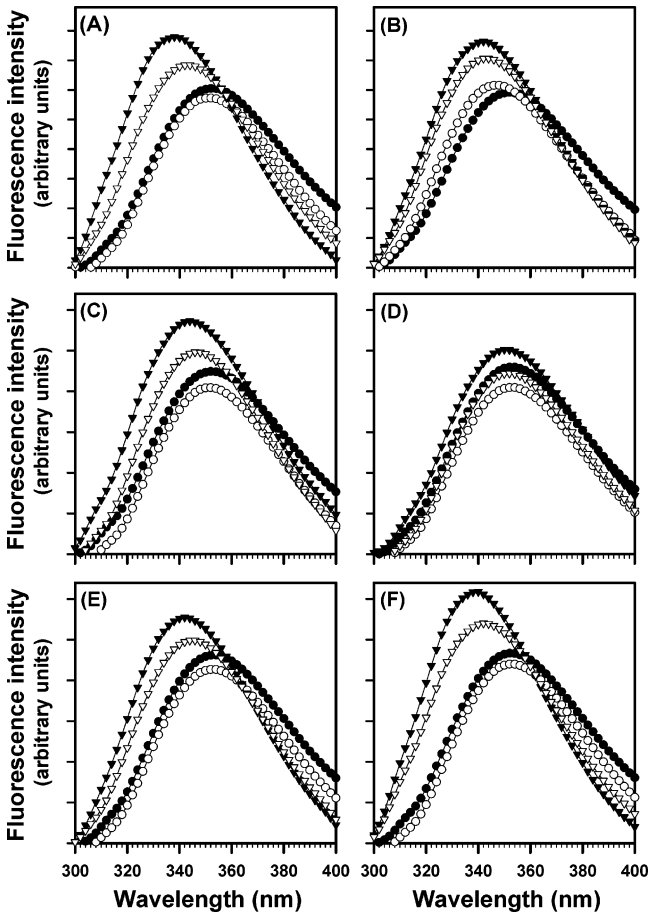

FIGURE 4: Trp fluorescence emission spectra. The final concentration of the peptides was 3 μM in the absence (●) or presence of liposomes composed of POPC (▽), POPC/POPG (2:1) (○), or POPG (▼) at a molar peptide/lipid ratio of 1:100: PMAP-23 (A); PMAP-PA (B); NF-PMAP (C); CF-PMAP (D); PMAP-W_7F_{21} (E); PMAP-F_7W_{21} (F). Data are representative of three independent experiments.

Table 2: Tryptophan Fluorescence Emission Maxima (nm) for PMAP-23 and Its Analogues in Tris Buffer with and without POPC, POPC/POPG (2:1), or POPG Liposomes at a Peptide/Lipid Molar Ratio of 1:100

peptides	Tris buffer	POPC	POPC/POPG (2:1)	POPG
PMAP-23	352	351 (1)[a]	344 (8)	339 (13)
PMAP-PA	352	347 (5)	343 (9)	342 (10)
NF-PMAP	353	353 (0)	347 (6)	345 (8)
CF-PMAP	353	353 (0)	351 (2)	350 (3)
PMAP-W_7F_{21}	352	351 (1)	345 (7)	342 (10)
PMAP-F_7W_{21}	352	351 (1)	343 (9)	338 (14)

[a] Blue shift of emission maxima compared to Tris buffer.

C-terminal helix inserts more deeply into the hydrophobic region of the phospholipid membrane than Trp^7 in the N-terminal helix.

Quenching Intrinsic Trp Fluorescence with Acrylamide. That the C-terminal region of PMAP-23 inserts more deeply into the membrane than the N-terminal part was confirmed by evaluating their accessibility to the neutral fluorescence quencher acrylamide in the presence and absence of the anionic liposomes. Stern−Volmer plots characterizing the quenching of Trp fluorescence in the absence and presence of POPC/POPG (2:1) liposomes are depicted in Figure 5 along with the apparent K_{SV} values. In buffer, increasing the

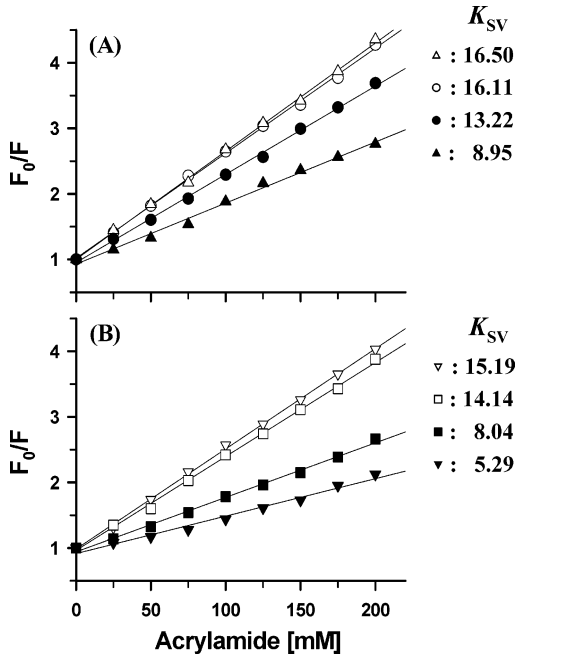

FIGURE 5: Stern−Volmer plots and constants (K_{SV}). Assays of single Trp-containing peptides were carried out in buffer with and without POPC/POPG (2:1) liposomes. The concentrations of peptides and liposomes were 3.0 and 300 μM, respectively. Symbols: NF-PMAP (△ and ▲); CF-PMAP (○ and ●); PMAP-W_7F_{21} (□ and ■); PMAP-F_7W_{21} (▽ and ▼). Empty and filled symbols indicate the absence and presence of the liposomes, respectively. Each data point is the mean of three independent experiments.

acrylamide concentration caused efficient quenching of the fluorescence of both helical fragments (NF-PMAP and CF-PMAP) and the single Trp analogues (PMAP-W_7F_{21}, PMAP-F_7W_{21}), as indicated by the linear increase in the F_0/F ratio (Figure 5A,B, open symbols). This is consistent with the expected accessibility of the Trp residues to acrylamide when the peptides are dissolved in buffer. On the other hand, in the presence of the anionic liposomes, the quenching of NF-PMAP is somewhat diminished, indicating the Trp residue to be in the lipid phase and thus less accessible to acrylamide, whereas CF-PMAP showed a minor reduction in quenching, indicating only a C-terminal fragment could not insert into the lipid bilayer. In contrast, the Trp^{21} residue of PMAP-F_7W_{21} was less accessible to the quencher than the Trp^7 residue of PMAP-W_7F_{21}, suggesting the C-terminus of PMAP-23 is more deeply buried in the hydrophobic interior than the N-terminus.

SPR Analysis of Peptide−Membrane Binding. Finally, we examined the binding of PMAP-23 and PMAP-PA to POPC/POPG (2:1) liposomes immobilized on a L1 sensor chip (Figure 6). When fitting the sensorgrams using different peptide concentrations, a two-state reaction model yielded a better fit than a simple 1:1 Langmuir binding model, revealing the interaction of the peptide with lipid bilayers to be a two-step process (initial binding and insertion). Therefore, kinetic analysis of the biosensor interactions was carried out using a two-state model that had been used previously to monitor the real-time interaction of two other membrane-active antimicrobial peptides, magainin II and melittin (*24*, *25*). The dotted lines in Figure 6 are the fitted sensorgrams obtained using the two-state model with the rate and affinity constants listed in Table 3; the solid lines are

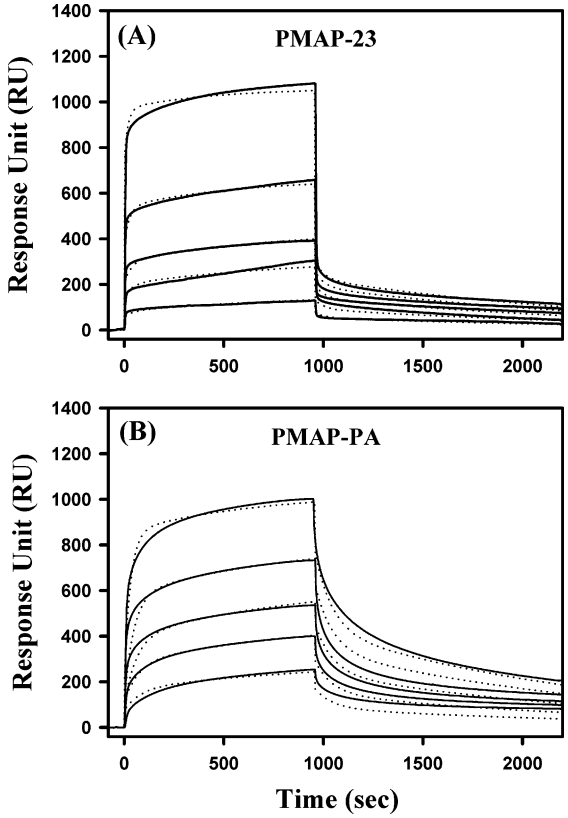

FIGURE 6: Sensorgrams for PMAP-23 and PMAP-PA binding to POPC/POPG (2:1) liposomes immobilized on L1 sensor chip surfaces. Overlay plot of the experimental (solid line) and calculated (dot line) sensorgrams using a two-state model. The peptide concentrations used were 3.125, 6.25, 12.5, 25, and 50 μM. Injections were made at time = 0 s; phosphate buffer was added to initiate dissociation at 980 s. Data are representative of two independent experiments.

the experimental data. The sensorgrams for the binding of PMAP-23 and PAMP-PA with POPC/POPG (2:1) showed similar response levels, indicating that the peptides have similar affinities for the lipid bilayer. Furthermore, there was little difference between the association (k_{a1}) and dissociation (k_{d1}) rate constants characterizing the initial binding of PMAP-23 and PMAP-PA to the membrane. The major difference between the peptides was observed in the subsequent insertion process; i.e., the association (k_{a2}) and dissociation (k_{d2}) rates of PMAP-23 were much faster than those of PMAP-PA, which again underscores the significance of the contribution made by the PXXP motif to the insertion of the C-terminal region into the hydrophobic interior of the lipid bilayer.

DISCUSSION

The nonspecific binding of antimicrobial peptides to negatively charged membranes depends on both electrostatic and hydrophobic interactions. Their amphipathic nature enables these peptides to selectively interact with and disrupt a variety of negatively charged microbial membranes, resulting in wide-spectrum antibiotic activity with little or no mammalian cell toxicity. Among these peptides, PMAP-23 adopts a highly amphipathic helix-hinge-helix structure in membrane mimetic environments. Disruption of the central hinge PXXP motif by Pro→Ala substitution significantly increased the α-helical content of the peptide, but reduced its antimicrobial potency and increases its hemolytic activity. In addition, interaction with zwitterionic liposomes had a negligible effect on Trp fluorescence of PMAP-23, but interaction with anionic liposomes elicited a very large blue shift and an increase in fluorescence quantum yield, indicating that PMAP-23 selectively binds to and disrupts anionic membranes. It is thus suggested that the hinge PXXP motif is crucial for the selective and effective antimicrobial activity of PMAP-23, probably because it enables optimal amphipathic distribution of the two helical parts of the peptide. In that regard, the N-terminal half of PMAP-23 showed stronger binding to anionic phospholipids than the C-terminal half, suggesting the N-terminal half mediates the initial electrostatic binding to the anionic membrane. In addition, the C-terminal half of the full peptide contains a short α-helical structure while the C-terminal fragment has a disordered structure, suggesting that the initial interaction of the N-terminal with the membrane proceeds to elongation of the C-terminal α-helix. Thus, it appears that the entire length of PMAP-23 is required for full antimicrobial effect, with the three parts acting in a cooperative manner to modulate the peptide's action.

To gain additional insight into the mechanism of action of PMAP-23, we prepared two single Trp analogues (PMAP-W_7F_{21} and PMAP-F_7W_{21}) with which to determine the orientation of the interacting peptide relative to the membrane. We found that the antibiotic activity, conformation and membrane disrupting properties of PMAP-W_7F_{21} and PMAP-F_7W_{21} were nearly identical to those of native PMAP-23. In anionic membranes, the Trp fluorescence from PMAP-F_7W_{21} was quenched less efficiently than that of PMAP-W_7F_{21}, indicating that the Trp residue in the C-terminal helix was located in a more hydrophobic environment than that of the N-terminal helix; i.e., the C-terminal helix inserts more deeply into the hydrophobic interior of lipid bilayer. To keep the N-terminal helix at the interface and to enable C-terminal insertion into the region of the hydrophobic acyl chains would require considerable flexibility in the central region. Similarly, it was previously reported that Pro residue favored the domain swapping in the P13Suc1 protein (*26*−*28*). Undoubtedly, thus, the conformational flexibility of the PXXP motif facilitates the hydrophobic interaction of the C-terminal helix with lipid bilayers. Previously, we found that the C-terminal region of PMAP-23 undergoes a structural change in membrane-mimetic environments (*20*) and that Trp^{21} is important for anchoring the C-terminal on phospholipid membranes (*19*). In the context of these earlier findings, our present observations are fully consistent with the proposed model in which PMAP-23 binds to target cell membranes in a two-step process (Figure 7). The peptide, which is unstructured in aqueous solution, initially adopts an amphipathic α-helical structure with the aid of electrostatic interactions between the cationic N-terminal helix and the anionic phospholipid headgroups and localizes to the membrane surface. In the second step, the peptide reorients itself − i.e., the C-terminal part of the peptide is inserted into the nonpolar interior of the lipid bilayer after Trp^{21} is anchored to the membrane surface. The central hinge PXXP motif, which is thought to be capable of both twisting and kinking (*29*), is essential for the insertion of PMAP-23 into the lipid bilayer. SPR analysis enabled us to clearly distinguish between the membrane binding and insertion steps. Interest-

Table 3: Association (k_{a1}, k_{a2}) and Dissociation (k_{d1}, k_{d2}) Kinetic Rate Constants for PMAP-23 and PMAP-PA Interacting with the POPC/POPG (2:1) Based on Numerical Integration Using a Two-State Reaction Model[a]

peptide	k_{a1} (1/Ms)	k_{d1} (1/s)	k_{a2} (1/s)	k_{d2} (1/s)	K (1/M)
PMAP-23	137 (±4.2)	80 (±5.3) × 10^{-4}	794 (±60.4) × 10^{-4}	67 (±5.0) × 10^{-4}	20.1 × 10^4
PMAP-PA	426 (±8.3)	104 (±7.9) × 10^{-4}	11.2 (±0.9) × 10^{-4}	7.4 (±0.6) × 10^{-4}	6.1 × 10^4

[a] The affinity constant (K) was determined as (k_{a1}/k_{d1})(k_{a2}/k_{d2}).

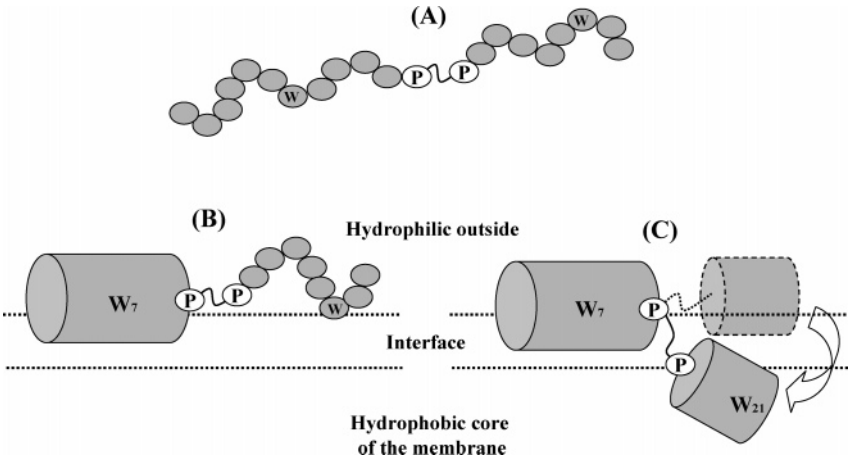

FIGURE 7: Proposed model for the interaction of PMAP-23 with a target cell membrane. (A) In aqueous buffer, PMAP-23 has no specific secondary structures. (B) The cationic properties of the N-terminal part of PMAP-23 are responsible for the initial binding to anionic membranes, which enables the N-terminal half to adopt an amphipathic α-helical structure. (C) The anchoring of Trp^{21} to the membrane interface induces formation of a C-terminus α-helix, after which bending and/or swiveling of the flexible central hinge (PXXP sequence) enables the C-terminal α-helix to insert into the target cell membrane.

ingly, the sensorgrams showed that whereas the initial binding of PMAP-23 and PAMP-PA to POPC/POPG (2:1) was similar, there was a major difference between the peptides in the second step, confirming that the PXXP motif significantly contributes to the insertion process. The conformational changes that take place during insertion are still not precisely known, but cis−trans isomerization of the two Pro residues may be involved.

Many membrane-active α-helical peptides carry one or two Pro residues (sometimes Gly residues) at a central position and form helix−hinge−helix structures thought to play structurally and functionally important roles (*30*−*34*). The ion-channel-forming peptides alamethicin and melittin contain central GXXP and GXP motifs, respectively. These motifs appear to give the helical structure a degree of flexibility that enables the N-terminal parts of the peptides to penetrate deep into the hydrophobic region of the bilayer (*35*). These peptides subsequently form transmembrane helices and voltage-gated channels or pores (*36*, *37*), making it noteworthy that Pro containing motifs also play key structural and dynamic roles in transmembrane helices (*38*−*42*). For instance, in their investigation of K^+ channels Kerr et al. (*40*) found that the PVP motif of S6 provides flexibility about a central hinge that might be related to the gating of the channel. And using the antimicrobial cecropin A-magainin II hybrid peptide, Oh et al. (*41*) showed that its central GIG hinge sequence plays an important role in its antibiotic activity and likely enables the C-terminal helix to span the lipid bilayer. In addition, van Kan et al. (*42*) recently showed that two Gly residues in clavanin act as flexible hinges that facilitate insertion of the hydrophobic N-terminal end deeply into the bilayer. Consistent with that idea, the antimicrobial and cell penetrating peptide buforin II shows reduced antibiotic and translocation efficiency when the central Pro is removed or substituted (*32*, *43*). Many signal peptides also contain a helix breaking residue (Pro or Gly) and adopt a dynamic helix−break−helix conformation in membrane-mimetic environments (*44*). Furthermore, such helix breaking residues show a position-dependent effect, which raises the possibility that they make conformational contributions to topogenesis (*45*). Most internal viral fusion peptides also contain a Pro at or near the center of their sequences. For example, influenza virus hemagglutinin adopts a helix−hinge−helix structure, and inhibition of the hinge capability reduces fusion activity (*46*, *47*). Overall, the dynamic nature of these hinged peptides suggests that substantial conformational changes occur during insertion into and/or translocation across membranes, results in significant local membrane perturbation.

In general, disruption of the α-helical structure caused by either inclusion of several D-amino acids or a central Pro-containing hinge contributes to selective cytotoxicity (*48*−*52*). However, unlike central Pro-containing peptides, the destabilization caused by D-amino acids should prevent the diastereomers from inserting and forming a transmembrane pore (*53*). With alamethicin and melittin, for example, the hinge motif makes them α-helical channel-forming peptides, but incorporation of D-amino acids into the peptides changed their mechanism of action from barrel-stave to a carpet-like mechanism. Recently, Papo and Shai (*25*) reported that melittin inserts into the PC/Cho bilayers, whereas its diastereomer is surface-localized by using SPR with mono- and bilayer membranes. This is in good agreement with the different modes of action between melittin and its diastereomer in zwitterionic membranes.

Several cathelicidin-derived antimicrobial peptides, including BMAP-27, BMAP-28, indolicidin, tritrpticin, and the Pro/Arg-rich peptides (PR-39 and the bactenecins), contain a

PXXP or PXXXP motif. Such Pro-rich sequences containing a PXXP motif are thought to bind the SH3 domain. For example, PR-39, which adopts a polyproline II conformation with several PXXP motifs, is thought to act by binding to the SH3 domains of the NADPH oxidase subunits, thereby blocking assembly of a functional enzyme (*54*). In NIH3T3 cells, the 15-residue N-terminal segment of PR-39 crosses the plasma membrane and binds SH3 domain-containing proteins such as pl30cas (*55*). In the cases of indolicidin (*56*, *57*) and tritrpticin (*58*−*61*), Pro residues play key roles in their extended and/or turn structure, and appear to be involved in targeting intracellular molecules. Although little is known about the function of their PXXP motifs, it seems clear that they are involved in peptide translocation and/or penetration across membranes, where they can exert a secondary effect.

In conclusion, its highly amphipathic and dynamic helix-hinge-helix structure makes PMAP-23 a good model with which to study the structures and processes involved in peptide-membrane binding and insertion and the mechanism of selective antimicrobial and permeabilization properties. The mode of action of PMAP-23 is probably modulated by the cooperative function of its N- and C-helices and central hinge. Based on our analyses, the interaction of PMAP-23 with microbial membranes entails an initial electrostatic interaction between the cationic N-terminal part of the peptide with the anionic phospholipid headgroups in the target cell membranes. This is followed by the bending and/or swiveling of the central PXXP motif, which precedes insertion of the C-terminal into the lipid bilayer and membrane perturbation. It is also possible that the PXXP motif facilitates the translocation of PMAP-23 across the lipid bilayer, where it may interact with secondary targets.

ACKNOWLEDGMENT

We greatly thank Dr. K. Matsuzaki, Kyoto University, Japan, for assistance with the peptide-lipid interactions.

REFERENCES

1. Zasloff, M. (2002) Antimicrobial peptides of multicellular organisms, *Nature 415*, 389−395.
2. Boman, H. G. (1995) Peptide antibiotics and their role in innate immunity, *Annu. Rev. Immunol. 13*, 61−92.
3. Hancock, R. E., and Diamond, G. (2000) The role of cationic antimicrobial peptides in innate host defenses, *Trends Microbiol. 8*, 402−410.
4. Lehrer, R. I., Lichtenstein, A. K., and Ganz, T. (1993) Defensins: antimicrobial and cytotoxic peptides of mammalian cells, *Annu. Rev. Immunol. 11*, 105−128.
5. Zanetti, M., Gennaro, R., and Romeo, D. (1995) Cathelicidins: a novel protein family with a common proregion and a variable C-terminal antimicrobial domain, *FEBS Lett. 374*, 1−5.
6. Bals, R., and Wilson, J. M. (2003) Cathelicidins—a family of multifunctional antimicrobial peptides, *Cell. Mol. Life Sci. 60*, 711−720.
7. Nizet, V., Ohtake, T., Lauth, X., Trowbridge, J., Rudisill, J., Dorschner, R. A., Pestonjamasp, V., Piraino, J., Huttner, K., and Gallo, R. L. (2001) Innate antimicrobial peptide protects the skin from invasive bacterial infection, *Nature 414*, 454−457.
8. Lehrer, R. I., and Ganz, T. (2002) Cathelicidins: a family of endogenous antimicrobial peptides, *Curr. Opin. Hematol. 9*, 18−22.
9. Risso, A. (2000) Leukocyte antimicrobial peptides: multifunctional effector molecules of innate immunity, *J. Leukoc. Biol. 68*, 785−792.
10. Zanetti, M., Gennaro, R., Scocchi, M., and Skerlavaj, B. (2000) Structure and biology of cathelicidins, *Adv. Exp. Med. Biol. 479*, 203−218.
11. Ramanathan, B., Davis, E. G., Ross, C. R., and Blecha, F. (2002) Cathelicidins: microbicidal activity, mechanisms of action, and roles in innate immunity, *Microbes Infect. 4*, 361−372.
12. Nicolas, P. and Mor, A. (1995) Peptides as weapons against microorganisms in the chemical defense system of vertebrates, *Annu. Rev. Microbiol. 49*, 277−304.
13. Shai, Y. (1999) Mechanism of the binding, insertion and destabilization of phospholipid bilayer membranes by alpha-helical antimicrobial and cell non-selective membrane-lytic peptides, *Biochim. Biophys. Acta 1462*, 55−70.
14. Epand, R. M., and Vogel, H. J. (1999) Diversity of antimicrobial peptides and their mechanisms of action, *Biochim. Biophys. Acta 1462*, 11−28.
15. Oren, Z., and Shai, Y. (1998) Mode of action of linear amphipathic alpha-helical antimicrobial peptides, *Biopolymers 47*, 451−463.
16. Matsuzaki, K. (1999) Why and how are peptide-lipid interactions utilized for self-defense? Magainins and tachyplesins as archetypes, *Biochim. Biophys. Acta 1462*, 1−10.
17. Lohner, K., and Prenner, E. J. (1999) Differential scanning calorimetry and X-ray diffraction studies of the specificity of the interaction of antimicrobial peptides with membrane-mimetic systems, *Biochim. Biophys. Acta 1462*, 141−156.
18. Zanetti, M., Storici, P., Tossi, A., Scocchi, M., and Gennaro, R. (1994) Molecular cloning and chemical synthesis of a novel antimicrobial peptide derived from pig myeloid cells, *J. Biol. Chem. 269*, 7855−7858.
19. Kang, J. H., Shin, S. Y., Jang, S. Y., Kim, K. L., and Hahm, K. S. (1999) Effects of tryptophan residues of porcine myeloid antibacterial peptide PMAP-23 on the antibiotic activity, *Biochem. Biophys. Res. Commun. 264*, 281−286.
20. Park, K., Oh, D., Shin, S. Y., Hahm, K. S., and Kim, Y. (2002) Structural studies of porcine myeloid antibacterial peptide PMAP-23 and its analogues in DPC micelles by NMR spectroscopy, *Biochem. Biophys. Res. Commun. 290*, 204−212.
21. Lee, D. G., Kim, D. H., Park, Y., Kim, H. K., Kim, H. N., Shin, Y. K., Choi, C. H., and Hahm, K. S. (2001) Fungicidal effect of antimicrobial peptide, PMAP-23, isolated from porcine myeloid against Candida albicans, *Biochem. Biophys. Res. Commun. 282*, 570−574.
22. Merrifield, R. B. (1986) Solid-phase synthesis, *Science 232*, 341−347.
23. Morton, T. A., Myszka, D. G., and Chaiken, I. M. (1995) Interpreting complex binding kinetics from optical biosensors: a comparison of analysis by linearization, the integrated rate equation, and numerical integration, *Anal. Biochem. 227*, 176−185.
24. Mozsolits, H., and Aguilar, M. I. (2002) Surface plasmon resonance spectroscopy: an emerging tool for the study of peptide-membrane interactions, *Biopolymers 66*, 3−18.
25. Papo, N., and Shai, Y. (2003) Exploring peptide membrane interaction using surface plasmon resonance: differentiation between pore formation versus membrane disruption by lytic peptides, *Biochemistry 42*, 458−466.
26. Rousseau, F., Schymkowitz, J. W., Wilkinson, H. R., and Itzhaki, L. S. (2001) Three-dimensional domain swapping in p13suc1 occurs in the unfolded state and is controlled by conserved proline residues, *Proc. Natl. Acad. Sci. U.S.A. 98*, 5596−5601.
27. Botos, I., Mori, T., Cartner, L. K., Boyd, M. R., and Wlodawer, A. (2002) Domain-swapped structure of a mutant of cyanovirin-N, *Biochem. Biophys. Res. Commun. 294*, 184−190.
28. Odaert, B., Landrieu, I., Dijkstra, K., Schuurman-Wolters, G., Casteels, P., Wieruszeski, J. M., Inze, D., Scheek, R., and Lippens, G. (2002) Solution NMR study of the monomeric form of p13suc1 protein sheds light on the hinge region determining the affinity for a phosphorylated substrate, *J. Biol. Chem. 277*, 12375−12381.
29. Sansom, M. S., and Weinstein, H. (2000) Hinges, swivels and switches: the role of prolines in signaling via transmembrane alpha-helices, *Trends Pharmacol. Sci. 21*, 445−451.
30. Zhang, L., Benz, R., and Hancock, R. E. (1999) Influence of proline residues on the antibacterial and synergistic activities of alpha-helical peptides, *Biochemistry 38*, 8102−8111.
31. Cordes, F. S., Bright, J. N., and Sansom, M. S. (2002) Proline-induced distortions of transmembrane helices, *J. Mol. Biol. 323*, 951−960.
32. Park, C. B., Yi, K. S., Matsuzaki, K., Kim, M. S., and Kim, S. C. (2000) Structure−activity analysis of buforin II, a histone H2A-

derived antimicrobial peptide: the proline hinge is responsible for the cell-penetrating ability of buforin II, *Proc. Natl. Acad. Sci. U.S.A. 97*, 8245−8250.
33. Tack, B. F., Sawai, M. V., Kearney, W. R., Robertson, A. D., Sherman, M. A., Wang, W., Hong, T., Boo, L. M., Wu, H., Waring, A. J., and Lehrer, R. I (2002) SMAP-29 has two LPS-binding sites and a central hinge, *Eur. J. Biochem. 269*, 1181−1189.
34. Ibrahim, H. R., Thomas, U., and Pellegrini, A. (2001) A helix-loop-helix peptide at the upper lip of the active site cleft of lysozyme confers potent antimicrobial activity with membrane permeabilization action, *J. Biol. Chem. 276*, 43767−43774.
35. Biggin, P. C., and Sansom, M. S. (1999) Interactions of alpha-helices with lipid bilayers: a review of simulation studies, *Biophys. Chem. 76*, 161−183.
36. Kaduk, C., Duclohier, H., Dathe, M., Wenschuh, H., Beyermann, M., Molle, G., and Bienert M. (1997) Influence of proline position upon the ion channel activity of alamethicin, *Biophys. J. 72*, 2151−2159.
37. Jacob, J., Duclohier, H., and Cafiso, D. S. (1999) The role of proline and glycine in determining the backbone flexibility of a channel-forming peptide, *Biophys. J. 76*, 1367−1376.
38. Lu, H., Marti, T., and Booth, P. J. (2001) Proline residues in transmembrane alpha helices affect the folding of bacteriorhodopsin, *J. Mol. Biol. 308*, 437−46.
39. Tieleman, D. P., Shrivastava, I. H., Ulmschneider, M. R., and Sansom, M. S. (2001) Proline-induced hinges in transmembrane helices: possible roles in ion channel gating, *Proteins 44*, 63−72.
40. Kerr, I. D., Son, H. S., Sankararamakrishnan, R., and Sansom, M. S. (1996) Molecular dynamics simulations of isolated transmembrane helices of potassium channels, *Biopolymers 39*, 503−515.
41. Oh, D., Shin, S. Y., Lee, S., Kang, J. H., Kim, S. D., Ryu, P. D., Hahm, K. S., and Kim, Y. (2000) Role of the hinge region and the tryptophan residue in the synthetic antimicrobial peptides, cecropin A(1−8)-magainin 2(1−12) and its analogues, on their antibiotic activities and structures, *Biochemistry 39*, 11855−11864.
42. van Kan, E. J., van der Bent, A., Demel, R. A., and de Kruijff, B. (2001) Membrane activity of the peptide antibiotic clavanin and the importance of its glycine residues, *Biochemistry 40*, 6398−6405.
43. Kobayashi, S., Takeshima, K., Park, C. B., Kim, S. C., and Matsuzaki, K. (2000) Interactions of the novel antimicrobial peptide buforin 2 with lipid bilayers: proline as a translocation promoting factor, *Biochemistry 39*, 8648−8654.
44. Chupin, V., Killian, J. A., Breg, J., de Jongh, H. H., Boelens, R., Kaptein, R., and de Kruijff, B. (1995) PhoE signal peptide inserts into micelles as a dynamic helix-break-helix structure, which is modulated by the environment. A two-dimensional 1H NMR study, *Biochemistry 34*, 11617−11624.
45. Rosch, K., Naeher, D., Laird, V., Goder, V., and Spiess, M. (2000) The topogenic contribution of uncharged amino acids on signal sequence orientation in the endoplasmic reticulum, *J. Biol. Chem. 275*, 14916−14922.
46. Hsu, C. H., Wu, S. H., Chang, D. K., and Chen, C. (2002) Structural characterizations of fusion peptide analogs of influenza virus hemagglutinin. Implication of the necessity of a helix-hinge-helix motif in fusion activity, *J. Biol. Chem. 277*, 22725−22733.
47. Delos, S. E., Gilbert, J. M., and White, J. M. (2000) The central proline of an internal viral fusion peptide serves two important roles, *J. Virol. 74*, 1686−1693.
48. Papo, N., Oren, Z., Pag, U., Sahl, H. G., and Shai, Y. (2002) The consequence of sequence alteration of an amphipathic alpha-helical antimicrobial peptide and its diastereomers, *J. Biol. Chem. 277*, 33913−33921.
49. Song, Y. M., Yang, S. T., Lim, S. S., Kim, Y., Hahm, K. S., Kim, J. I., and Shin, S. Y. (2004) Effects of L- or D-Pro incorporation into hydrophobic or hydrophilic helix face of amphipathic alpha-helical model peptide on structure and cell selectivity, *Biochem. Biophys. Res. Commun. 314*, 615−621.
50. Shin, S. Y., Lee, S. H., Yang, S. T., Park, E. J., Lee, D. G., Lee, M. K., Eom, S. H., Song, W. K., Kim, Y., Hahm, K. S., and Kim, J. I. (2001) Antibacterial, antitumor and hemolytic activities of α-helical antibiotic peptide, P18 and its analogs, *J. Peptide Res. 58*, 504−514.
51. Pukala, T. L., Brinkworth, C. S., Carver, J. A., and Bowie, J. H. (2004) Investigating the importance of the flexible hinge in caerin 1.1: solution structures and activity of two synthetically modified caerin peptides, *Biochemistry 43*, 937−944.
52. Chia, B. C., Carver, J. A., Mulhern, T. D., and Bowie, J. H. (2000) Maculatin 1.1, an anti-microbial peptide from the Australian tree frog, Litoria genimaculata solution structure and biological activity, *Eur. J. Biochem. 267*, 1894−1908.
53. Papo, N., and Shai, Y. (2004) Effect of drastic sequence alteration and D-amino acid incorporation on the membrane binding behavior of lytic peptides, *Biochemistry 43*, 6393−6403.
54. Shi, J., Ross, C. R., Leto, T. L., and Blecha, F. (1996) PR-39, a proline-rich antibacterial peptide that inhibits phagocyte NADPH oxidase activity by binding to Src homology 3 domains of p47 phox, *Proc. Natl. Acad. Sci. U.S.A. 93*, 6014−6018.
55. Chan, Y. R., and Gallo, R. L. (1998) PR-39, a syndecan-inducing antimicrobial peptide, binds and affects p130(Cas), *J. Biol. Chem. 273*, 28978−28985.
56. Falla, T. J., Karunaratne, D. N., and Hancock, R. E. (1996) Mode of action of the antimicrobial peptide indolicidin, *J. Biol. Chem. 271*, 19298−19303.
57. Rozek, A., Friedrich, C. L., and Hancock, R. E. (2000) Structure of the bovine antimicrobial peptide indolicidin bound to dodecylphosphocholine and sodium dodecyl sulfate micelles, *Biochemistry 39*, 15765−15774.
58. Schibli, D. J., Hwang, P. M., and Vogel, H. J. (1999) Structure of the antimicrobial peptide tritrpticin bound to micelles: a distinct membrane-bound peptide fold, *Biochemistry 38*, 16749−16755.
59. Yang, S. T., Shin, S. Y., Kim, Y. C., Kim, Y., Hahm, K. S., and Kim, J. I. (2002) Conformation-dependent antibiotic activity of tritrpticin, a cathelicidin-derived antimicrobial peptide, *Biochem. Biophys Res. Commun. 296*, 1044−1050.
60. Nagpal, S., Gupta, V., Kaur, K. J., and Salunke, D. M. (1999) Structure−function analysis of tritrypticin, an antibacterial peptide of innate immune origin, *J. Biol. Chem. 274*, 23296−23304.
61. Yang, S. T., Shin, S. Y., Lee, C. W., Kim, Y. C., Hahm, K. S., and Kim, J. I. (2003) Selective cytotoxicity following Arg-to-Lys substitution in tritrpticin adopting a unique amphipathic turn structure, *FEBS Lett. 540*, 229−233.

BI051524K